Decomposition-Based Assembly Synthesis of Space Frame Structures Using Joint Library

Naesung Lyu

Kazuhiro Saitou[1]
e-mail: kazu@umich.edu

Department of Mechanical Engineering,
University of Michigan,
Ann Arbor, MI 48109-2125

This paper presents a method for identifying the optimal designs of components and joints in the space frame body structures of passenger vehicles considering structural characteristics, manufacturability, and assembleability. Dissimilar to our previous work based on graph decomposition, the problem is posed as a simultaneous determination of the locations and types of joints in a structure and the cross sections of the joined structural frames, selected from a predefined joint library. The joint library is a set of joint designs containing the geometry of the feasible joints at each potential joint location and the cross sections of the joined frames, associated with their structural characteristics as equivalent torsional springs obtained from the finite element analyses of the detailed joint geometry. Structural characteristics of the entire structure are evaluated by finite element analyses of a beam-spring model constructed from the selected joints and joined frames. Manufacturability and assembleability are evaluated as the manufacturing and assembly costs estimated from the geometry of the components and joints, respectively. The optimization problem is solved by a multiobjective genetic algorithm using a direct crossover. A case study on an aluminum space frame of a midsize passenger vehicle is discussed. [DOI: 10.1115/1.1909203]

Keywords: design for manufacturing, assembly synthesis, structural design, aluminum space frame

1 Introduction

Although often ideal from a structural viewpoint, monolithic designs are not a realistic solution for complex structures, such as automotive bodies, considering the cost-effectiveness of manufacturing processes. As a result, most structural products are designed as assemblies of components with simpler geometries. During the conceptual stage of such products, designers need to determine the set of components and the methods of joining the components, by decomposing the entire product geometry. In the automotive industry, for example, a handful of basic decomposition schemes considering geometry, functionality, and manufacturing issues have been used in this process. However, these decomposition schemes depend mainly on the designers' experience, which may cause the following problems directly related to the component and joint configurations:

- *Insufficient structural stiffness*. Components and joining methods specified by designers cannot meet the desired stiffness of the final assembly because of the inappropriate allocation of joints, which are less stiff than components.
- *Insufficient manufacturability*. Components and joining methods specified by designers cannot be economically manufactured because of the inappropriate geometry in components and joints.

Therefore, a cost-effective and systematic optimization method, which can be used in determining components set by considering overall structural characteristics, manufacturability, and assembleability, will be of significant impact on the industry. As such, this paper presents a method for identifying the optimal designs of components and joints in space frame body structures of passenger vehicles, considering structural characteristics, manufacturability, and assembleability.

Dissimilar to our previous work based on graph decomposition [1,2], the problem is posed as a simultaneous determination of the locations and types of joints in a structure and the cross sections of the joined structural frames, selected from a predefined joint library [3]. The joint library is a set of joint designs containing the geometry of the feasible joints at each potential joint location and the cross sections of the joined frames, associated with their structural characteristics as equivalent torsional springs obtained from the finite element analyses (FEA) of the detailed joint model made of solid and plate elements. To minimize the computational overhead during optimization, the artificial neural network (ANN) associated with the FEA analyses results [4,5] is built for each configuration type in the joint library by using sampled designs of feasible joints and joined frames [6] and utilized in the overall optimization problem.

Structural characteristics of the entire structure are evaluated by the finite element analyses of a model made of beam elements (frames) and torsional spring elements (joints), constructed from the selected joints and joined frames. Manufacturability of components is evaluated based on the estimated manufacturing cost consisting of the costs of extrusion die, bending operation, and casting component for each joint. Assembleability is estimated by the cost of welding in the assembly process. The optimization problem is solved by a multiobjective genetic algorithm [7] using a direct crossover [8,9]. A case study on an ASF of a mid-size passenger vehicle is discussed.

2 Related Work

2.1 DFA/DFM and Assembly Synthesis. Design for assembly (DFA) and design for manufacturing (DFM) refers to a collection of design methods that aim to identify and alleviate manufacturing and assembly problems at the product design stage. Boothroyd and Dewhurst [10], who are regarded as major estab-

[1]Corresponding author.

Contributed by the Design Engineering Division of ASME for publication in the JOURNAL OF MECHANICAL DESIGN. Manuscript received June 13, 2004; final manuscript received November 25, 2004. Assoc. Editor: K.K. Choi.

lishers of DFA/DFM concepts, suggest to reducing part count first, followed by part redesign to improve manufacturability and assembleability [11]. The analyses of manufacturability and assembleability require a targeting product to be decomposed into elementary manufacturing and assembly features, such as surfaces, dimensions, tolerances, and their correlations [12]. Therefore, the conventional DFA/DFM methods assume predetermined components with given geometries and suggests improvements by modifying the given geometries.

Decomposition-based assembly synthesis [1,2,9,13,14] adopted in this paper, on the other hand, emphasizes the determination of components prior to the manufacturability and assembleability analyses. The method starts with no prescribed components and generates an optimal component set considering the properties, including structural characteristics of the assembled product, manufacturability, and assembleability.

2.2 Automotive Body Structure Modeling. During the early design stage of automotive body-in-white (BIW), simple beam models are widely used. Although beam elements can reasonably model structural members, difficulties often arise in modeling the structural property of joints. Modeling joints as torsional springs [15] is a classic but popular method because of its simplicity, where equivalent torsional spring rates are identified from experiments or detailed FEA models made of shell elements. Lee and Nikolaidis [16] proposed a two-dimensional (2D) joint model in order to consider joint flexibility, the offset of rotation centers, and coupling effects between the movements of joint branches. Kim et al. [17] discussed the accuracy of FEA-based joint rate evaluations regarding transformation error from shell element model to spring rate and proposed their own model [18].

Aiming at joint design, Long [6] presented two tools that link the performance targets for a joint in a BIW to its geometry. The first tool, called translator A, predicts the structural performance of a given joint geometry using an artificial neural network (ANN) and response surface method (RSM). The second tool, called translator B, solves the inverse problem of finding a joint geometry that meets the given performance targets, using the translator A and sequential quadratic programing (SQP). Nishigaki et al. [19] proposed a tool based on first-order analysis (FOA) to design basic layouts of automotive structures, considering models of beam and spring elements. The above works, however, are on the analyses of structural properties of joints, separately or as an integral of an overall structure, and do not addresses the automated synthesis of joint locations and designs within a BIW as addressed in this paper.

2.3 Aluminum Space Frame (ASF) Design. During the last two decades aluminum has drawn significant attention from the automotive industry because of the increasing demands on high-gas-mileage, lightweight, and environmentally friendly vehicles. Although aluminum has been successfully used in drivetrains and heat exchangers, its usage in the chassis and body is still under development. Since a body-in-white (BIW) accounts for approximately one third of the vehicle weight, much effort has been put on the adaptation of aluminum in BIW [20–23], resulting in a number of commercial mass-produced vehicles with the ASF, such as Acura's NSX [24], Audi's A2 and A8 [25] (see Fig. 1), and BMW's Z8 [26]. Ahmetoglu [27] discussed the design of extruded profiles, bending, friction and formability of aluminum components. Chung et al. [28] studied joint designs in the ASF by comparing FE models with experimental results. Powell and Wiemer [29] and Barnes and Pashby [30,31] summarized the joining technologies currently used in aluminum structure vehicles, including resistance spot welding (RSW), gas metal arc welding (GMAW), self-piercing joint, and laser welding. In the present paper, we are providing a way of finding optimized configurations of components in the ASF considering structural response, manufacturing, and assembly process.

Fig. 1 (*a*) Audi A2 and (*b*) ASF [20]

3 Approach

The proposed method consists of the following two steps (Fig. 2):

1. Geometry of a given structure is transformed into a structural topology graph that represents the liaisons between basic members, the smallest decomposable components of the given structure, identified by the potential joint locations specified by the user. For each potential joint location, a corresponding joint library is built.
2. The structural topology graph defined in the first step is decomposed, through an optimization process, into subgraphs representing components by assigning to some of the potential joint locations the joint types and cross sections of the joined frames, selected from the joint library. During this optimization process, the components set represented as the subgraphs is evaluated by considering (i) stiffness of the assembled structure, (ii) manufacturability of components and cast "sleeves" for joints, and (iii) assembleability of the components with the selected joints.

The rest of the section describes the details of the above steps with a sample space frame structure in Fig. 3. As illustrated in Fig. 3(*b*), it is assumed that frames are extruded tubes, bent or welded with cast "sleeves" at joints, following a typical construction method of AFS.

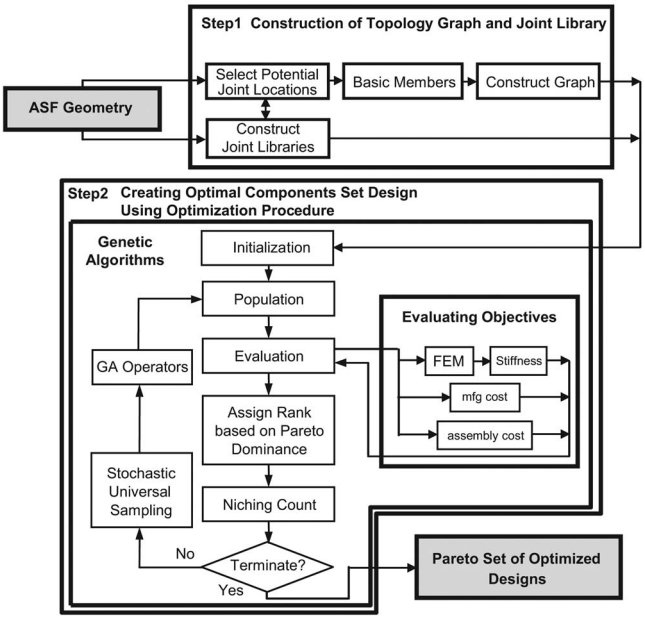

Fig. 2 Approaches used in this paper

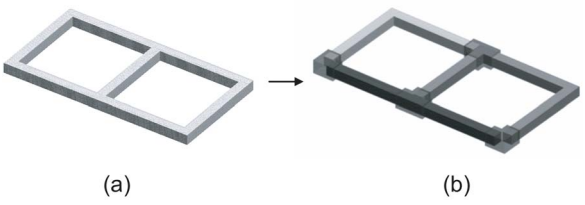

Fig. 3 (*a*) Sample space frame structure and (*b*) decomposed structure with joints (welded cast sleeves)

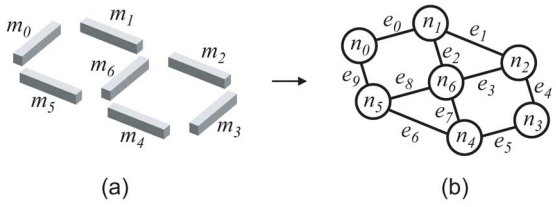

Fig. 5 (*a*) Seven basic members (m_0–m_6) and (*b*) structural topology graph with seven nodes (n_0–n_6) and ten edges (e_0–e_9)

3.1 Overview. Step 1: Construction of structural topology graph with joint libraries. Different from our previous approach [1,2] where the basic members are specified by the designer, the present method requires the designer to specify the potential joint locations. This is to guarantee that the final design contains only the joints feasible for the available frame manufacturing and joining methods.

Figure 4 illustrates an example of six potential joint locations shown as gray boxes. At each potential joint location, the designer must also specify feasible joint types to be included in the joint library. The joint library is a set of joint designs containing the geometric configurations (types) of the feasible joints, the cross-sectional dimensions of the joined frames, and the welding design at each potential joint location.

The joint library J_i of potential joint location i is defined as a triple

$$J_i = (T_i, S_i, W_i) \tag{1}$$

where T_i, S_i, and W_i are the set of the feasible geometric configuration types, the set of feasible cross sections of the intersecting frames, and the set of feasible welding designs, respectively, at potential joint location i. Since multiple frames intersect at a potential joint location, the elements $\mathbf{s}_i$ of S_i is a vector

$$\mathbf{s}_i \in FS_{FJ_i(0)} \times FS_{FJ_i(1)} \times \cdots \times FS_{FJ_i(nf_i)} \tag{2}$$

where FS_k is the set of valid beam cross section designs for frame k in the structure, FJ_i is the set of the intersecting frames at potential joint location i, and $|FJ_i| = nf_i$. For example, the joint library J_1 at the potential joint location **1** of Fig. 4 is T_1, S_1, W_1 with $T_1 = \{t_{1.0}, t_{1.1}, t_{1.2}, t_{1.3}\}$.

The structural property of a joint is determined by a joint configuration type, a cross-section design of the joined frames, and a weld design. As described in Section 3.2, an ANN is constructed for each joint configuration type, in order to represent the mapping between the joint design variables (cross section and weld designs) and its structural property (torsional spring rates).

With given potential joint locations, basic members in the structure can be identified as shown in Fig. 5(a). Then, the structural topology graph $G=(V,E)$ is constructed from basic members such that the basic member m_i is represented as node n_i in V, and the liaison between two basic members m_i and m_j is represented as edge $e=\{n_i, n_j\}$ in E.

Figure 5(b) illustrates the structural topology graph G with seven nodes corresponding to the seven basic members in Fig. 5(a) and ten edges connecting the adjacent nodes.

Step 2: Creating optimal components set design using optimization procedure. Different from our previous approach [1,2] where structural topology graph G is decomposed by removing its edges, the present method decomposes G by selecting a joint configuration type in the library at each potential joint location. From the selected joint configuration types, the corresponding edges in G are removed.

For example, by selecting joint configuration type $t_{1.2}$ in T_1 for the joint location **1** in Fig. 6, the corresponding edges $e_1 = \{n_1, n_2\}$ and $e_2 = \{n_1, n_6\}$ are removed. The motivation behind the new approach over the simple removal of edges (as in our previous work) is to establish one-to-one mapping between the topology of G and joint configuration designs. With the simple edge removal, multiple topologies of G can correspond to a joint configuration type. For example, all possible joint configuration types involving three frames (e.g., location **1** in Fig. 6) is 5, while number of possible graphs with three nodes is $2^{\text{number of edges}} = 2^3 = 8$. This is because the case where all three frames are connected

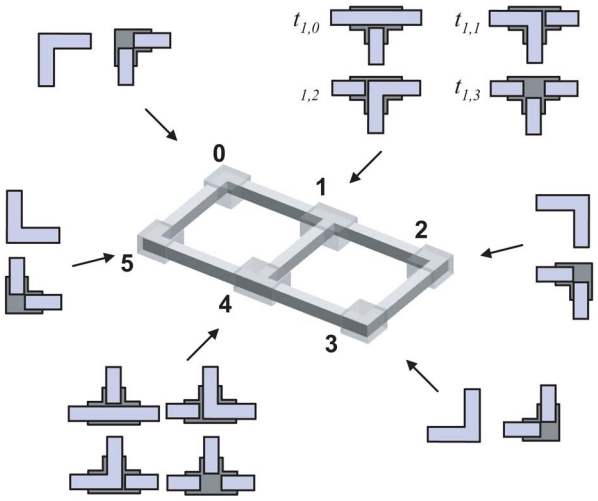

Fig. 4 Specified six potential joint locations (0–5, colored as gray boxes) and possible configurations (types) for each joint

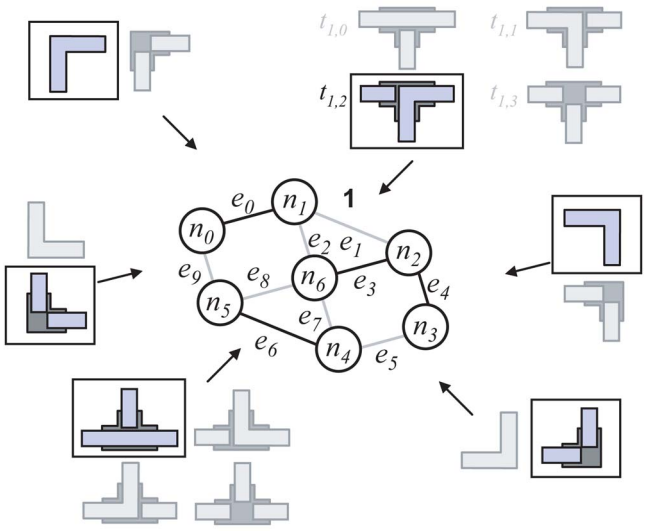

Fig. 6 Selected joint types and topology graph with the corresponding edges removed

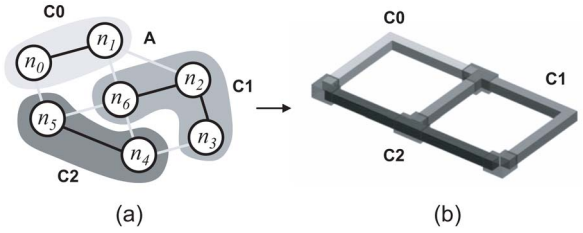

Fig. 7 (*a*) Three subgraphs and (*b*) corresponding three components

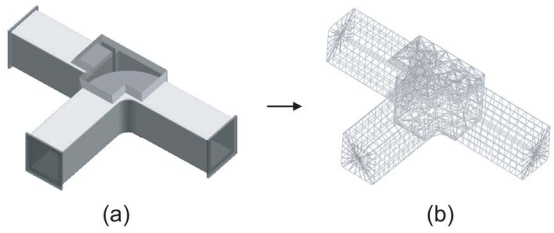

Fig. 9 (*a*) Detailed 3D solid model of a joint and (*b*) its FE model with plate elements for beams, solid elements for casting, and plate elements for welding

can be represented by four different topologies in the graph. The simple edge removal, therefore, often yields overly connected components, which can be prevented by using the new approach above.

The selection of joint configuration types and the removal of the corresponding edges in G result in subgraphs of G, each of which corresponds to a component. The cross-sectional dimensions of a component are then set as the averages of the ones of the joining frames associated with the selected joint configuration types in the component, which are subsequently used for retrieving the precomputed structural properties of the joints from the joint library. Figure 6, for example, shows three subgraphs (Fig. 7(*a*)), and the corresponding components (Fig. 7(*b*)) resulted from the selection of the joint types in Fig. 6.

The optimal decomposed structures with component and joint designs are obtained using the decomposition procedures described above through an optimization loop for three objectives: (i) stiffness of the assembled structure, (ii) manufacturability of components and cast "sleeves" for joints, and (iii) assembleability of the components with the selected joint types.

3.1.1 Structural Stiffness. The structural stiffness of the assembled structure is evaluated as a negative of the magnitude of total displacements at specific locations of the assembled structure under given loading conditions. The displacements are calculated with finite element analyses, where the components and joints are represented by beam elements and torsional spring elements, respectively.

For example, a T-joint in Fig. 8(*a*) is modeled as three beam elements connected by torsional spring elements k_0, k_1, and k_2, each of which has torsional stiffness (rate) around three local orthogonal axes attached to the joint. Note that the relative translations of these elements are constrained. The section properties of the beam elements are obtained from the cross-sectional dimensions of the components. The rate of the torsion spring elements are estimated by the finite element analyses of the detailed model of a joint, where frames are modeled with plate elements, a cast "sleeve" is modeled as solid elements, and welds joining the frames and the sleeve are modeled as plate elements, as illustrated in Fig. 9.

Figure 10 illustrates the loading and boundary conditions for calculating torsional spring rates of in-plane rotation. To facilitate the load application and the measurement of distortion angles, a rigid beam element is added to the center of the frame, subject to rotation. In Fig. 10, distortion angles θ_0, θ_1, and θ_2 account for the effects of k_1 and k_2, k_0, and k_2, and k_0 and k_1, respectively, in Fig. 7. Assuming moment arm length L, which is measured as the distance from the rotational center to the point at which the loading P is applied, the following equations are used to estimate k_0, k_1, and k_2 for in-plane rotation:

$$k_{0,\text{in-plane}} = \frac{PL}{2}\left(-\frac{1}{\theta_0}+\frac{1}{\theta_1}+\frac{1}{\theta_2}\right)$$

$$k_{1,\text{in-plane}} = \frac{PL}{2}\left(\frac{1}{\theta_0}-\frac{1}{\theta_1}+\frac{1}{\theta_2}\right)$$

$$k_{2,\text{in-plane}} = \frac{PL}{2}\left(\frac{1}{\theta_0}+\frac{1}{\theta_1}-\frac{1}{\theta_2}\right) \tag{3}$$

The other two components of torsional spring rates are calculated in a similar manner. The values of the torsional spring rates for typical joint types, cross-sectional dimensions of the joined frames, and amount of welds are precomputed to produce a set of training data for an artificial neural network (ANN) that implements the joint library. Similar to the translator A's in [6], this approach allows the spring rates of a joint to simply be retrieved from the joint library without computational overheads during optimization.

3.1.2 Component Manufacturability. The manufacturability of components is evaluated as a negative of the total cost of producing components. As stated earlier, it is assumed that frames are extruded tubes, bent or welded with cast "sleeves" at joints, following a typical construction method of AFS. For example, the design in Fig. 11(*a*) is composed of three frames (Fig. 11(*b*)) and four cast sleeves (Fig. 11(*c*)). The cost of producing components is estimated by the sum of the cost of extrusion die (assumed as proportional to the size and complexity of the frame cross sections) and the cost of bending operations (assumed as proportional

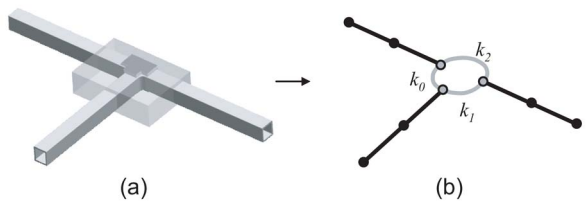

Fig. 8 (*a*) Frames with connected by a T-joint and (*b*) their FE model with beam elements (solid lines) and torsional spring elements (gray lines)

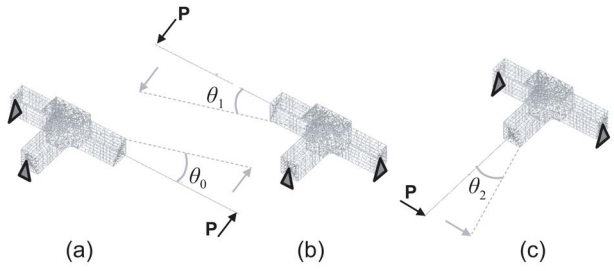

Fig. 10 Estimating torsional spring rates using FE analysis

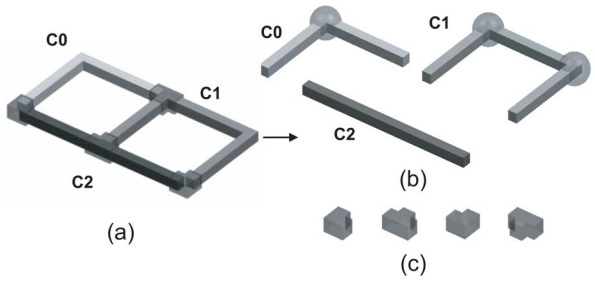

Fig. 11 (*a*) Sample design, (*b*) three components with three bends (shown as shaded spheres), and (*c*) four cast sleeves for joining

to the number of bending). The cost of producing cast sleeves is estimated by the cost of casting, which is assumed as simply proportional to its volume.

3.1.3 Component Assembleability. The assembleability of components is calculated as a negative of the total cost of joining. In this paper, the method of joining is assumed to be the GMAW, which is widely used for the ASF [27]. The welds are applied between the frames and the cast sleeves at joints. The cost is assumed to be proportional to the volume of total welds, which can be calculated from the total welding length multiplied by weld thickness.

3.2 Mathematical Formulation.

3.2.1 Definition of Design Variables. A design is uniquely specified by (i) the joint configuration types at all potential joint locations, (ii) the cross-sectional dimensions of all frames (basic members), and (iii) the welding designs at all joints, which are represented by the following three vectors $\mathbf{x}$, $\mathbf{y}$, and $\mathbf{z}$, respectively:

$$\mathbf{x} \in T_0 \times T_1 \times \cdots \times T_{n-1}$$

$$\mathbf{y} \in FS_0 \times FS_1 \times \cdots \times FS_{B-1}$$

$$\mathbf{z} \in W_0 \times W_1 \times \cdots \times W_{n-1} \tag{4}$$

where T_i is the set of feasible joint configuration types at potential joint location i (Eq. (1)), n is the number of the potential joint locations, FS_k is the set of valid beam cross-section a designs for frame k in the structure (Eq. (2)), B is the number of frames in the structure, and W_i is the set of valid welding designs at potential joint locations i (Eq. (1)). Note that in general, the elements of vectors $\mathbf{y}$ and $\mathbf{z}$ are also vectors depending on the definitions of beam cross-sectional designs and welding designs, as appeared in the following case study.

3.2.2 Definition of Objective Functions. Using the design variables $\mathbf{x}$, $\mathbf{y}$, and $\mathbf{z}$, the three objective functions described in Section 3.2.1 are given as follows:

$$f_{\text{stiff}}(\mathbf{x},\mathbf{y},\mathbf{z}) = -\,\text{DISP}[\text{XSEC}(\mathbf{x},\mathbf{y}),\text{JRATE}(\text{XSEC}(\mathbf{x},\mathbf{y}),\mathbf{z})] \tag{5}$$

$$f_{\text{mfg}}(\mathbf{x},\mathbf{y}) = -\sum_{i=0}^{n-1}\{\text{DIEC}(\text{COMP}(i,\mathbf{x}),\mathbf{y}) + \text{BNDC}(\text{COMP}(i,\mathbf{x}))\} - \sum_{i=0}^{m-1}\text{CASTC}(i,\mathbf{x}) \tag{6}$$

$$f_{\text{assm}}(\mathbf{z}) = -\,C_w\sum_{i=0}^{m-1}\text{WLDL}(i,\mathbf{z}) \times \text{WLDT}(i,\mathbf{z}) \tag{7}$$

where n and m are the numbers of components and joints in a decomposes structure, respectively. DISP is the amount of displacements at predefined points of the beam-torsional spring FE model of assembled structure. $\text{XSEC}(\mathbf{x},\mathbf{y})$ are the cross-sectional properties of the components specified by $\mathbf{x}$ with the beam cross-sectional dimensions specified by $\mathbf{y}$. JRATE returns the torsional spring rates at each joint with the cross-sectional properties XSEC and welding design $\mathbf{z}$. This function is using the ANNs to mapping the design variables to the torsional spring rates. $\text{COMP}(i,\mathbf{x})$ is the ith component specified by $\mathbf{x}$. DIEC and BNDC are the cost of extrusion die and bending operation of a component, respectively. $\text{CASTC}(i,\mathbf{x})$ is the casting cost at the ith joint specified by $\mathbf{x}$. C_w is the cost of welding operation per unit weld volume. $\text{WLDL}(i,\mathbf{z})$ and $\text{WLDT}(i,\mathbf{z})$ are the length and thickness of the welds at the ith joint as specified by $\mathbf{z}$.

3.2.3 Formulation of Optimization Problem. Given the design variables and the objective functions as defined above, the following multiobjective optimization problem is formulated:

maximize: $\{f_{\text{stiff}}(\mathbf{x},\mathbf{y},\mathbf{z}), f_{\text{mfg}}(\mathbf{x},\mathbf{y}), f_{\text{assm}}(\mathbf{z})\}$

subject to: $\mathbf{x} \in T_0 \times T_1 \times \cdots \times T_{n-1}$

$\mathbf{y} \in FS_0 \times FS_1 \times \cdots \times FS_{B-1}$

$\mathbf{z} \in W_0 \times W_1 \times \cdots \times W_{n-1}$

Note that there is no explicit constraint in this problem.

A modified nondominated sorting genetic algorithm-II (NSGA-II) [7] is adopted for the above problem because of the discrete nature of the design variables and its ability to solve multiobjective problems without predefined weight or bounds. This ability also enables us to exclude the problems of normalizing or scaling objectives. Some enhancements to the conventional NSGA-II are made in the niching based on the distances in object function space and the stochastic universal sampling, which were successfully applied in our previous works [2].

A chromosome $\boldsymbol{c}$ (an internal representation of design variables for genetic algorithms) is a simple list of the three design variables:

$$\boldsymbol{c} = (\mathbf{x},\mathbf{y},\mathbf{z}) \tag{8}$$

Since the information in $\mathbf{x}$, $\mathbf{y}$, and $\mathbf{z}$ are linked to the geometry of structure, the conventional one- or multiple-point crossover for linear chromosomes [32] are ineffective in preserving high-quality building blocks. For this type of problem, direct crossover has been successfully applied to improve the performance [2,8,9]; details can be found in [2] along with the description of the modified NSGA-II.

4 Case Studies

This section presents a case study on a model of the ASF for a passenger vehicle shown in Fig. 12. The actual vehicle design (Fig. 12(*a*)) is first simplified (Fig. 12(*b*)), where all frames are assumed as square tubes with identical external dimensions and with possibly different internal thicknesses.

Since the actual vehicle body is a mixture of extruded and cast parts, only the portions corresponding to the extruded parts are subject to decomposition in the simplified model. Assuming symmetric components in the left and right sides of the body, the design variables are assigned to only one side of the simplified model. Table 1 shows the material properties used in this case study. Total of 30 possible joint locations are specified as shown in Fig. 13(*a*). These possible joint locations are classified into three types **A**, **B**, and **C**, each of which has feasible joint types shown

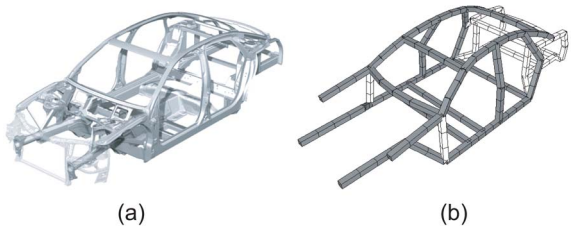

Fig. 12 (*a*) ASF for Audi A8 [20] and (*b*) simplified frame model used in the case study. Extruded and cast components are shaded dark and light, respectively.

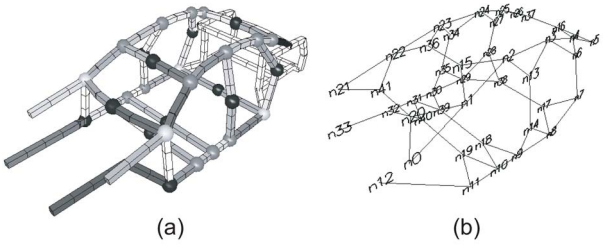

Fig. 14 (*a*) Resulting 42 basic members and (*b*) constructed structural topology graph with 42 nodes and 66 edges

in Fig. 13(*b*) with 90 or 180 degree angles between the joined frames. Location type **A** has two joint types **a0** and **a1**. In **a0**, beams 0 and 1 are one component ((0,1)) whereas in a1, beams 0 and 1 are welded with cast sleeve ((0),(1)). Location type **B** has three configuration designs **b0**, **b1**, and **b2**. In **b0**, beams 0 and 2 is one component, joined to 1 ((0,2),(1)). Similarly, **b1** and **b2** have two components ((0,1),(2)) and ((0),(1,2)), respectively. For location type **C**, **c0**, **c1**, and **c2** have joint types ((1,2),(0)), ((1),(0,2)), and ((0,1),(2)), respectively.

Based on the specified possible joint locations, 42 basic members are identified (Fig. 14(*a*)). The structural topology graph G with 42 nodes and 66 edges is constructed from the identified basic members (Fig. 14(*b*)). Figure 15 illustrates the definition of beam cross-section design variable and joining design variable. Note that the height and width of the cross section are not included as design variables. Considering the symmetricity, the variables are assigned only to the 21 basic members corresponding to the left half of the body structure.

Stiffness of the assembled structure is calculated considering the maximum displacement of the floor frame under bending loads (Fig. 16). The main loads of powertrain F_{pt}, the front passengers/seats F_{pf}, the rear passenger/seats F_{pr}, and the luggage F_l are only considered [33], where the magnitude of each load is the weight of the corresponding component multiplied by a dynamic load factor. The rear suspension locations are constrained in x, y, and z translations, while the front suspension locations are constrained in z (upward) translation only. Table 2 shows magnitude of the applied loads and the dynamic load factor.

As training data for the artificial neural network (ANN) that implements the joint library, the detailed three-dimensional (3D) models of 7 joint types (**a1**, **b0**–**b2**, **c0**–**c2**) in Fig. 13(*b*) are analyzed using finite element analyses. For joint type a1, three torsional spring rates (x, y, and z components between two joining frames) are calculated. For the other joint types, nine torsional spring rates (x, y, and z components among three joined frames as shown in Fig. 8) are calculated. For the joint types where the in-plane rotations are dominant, (**a1**, **b0**–**b2**), Eq. (3) is used for evaluating torsional spring rates. However, the other joint types **c0**–**c2** will require a different equation because it will result in off-plane rotations. In this case, Eq. (3) has been modified to match the torsional spring rates in the same rotational direction. In

Table 1 Material properties in the ASF model

Process	Name	E[a] (GPa)	Poisson ratio	Density (kg/m^3)
Extrusion	A6061-T6	70.5	0.33	2700.00
Casting	A356.0-T6	72.4	0.33	2685.00
Welding	A4043	70.5	0.33	2700.00

[a]Young's modulus

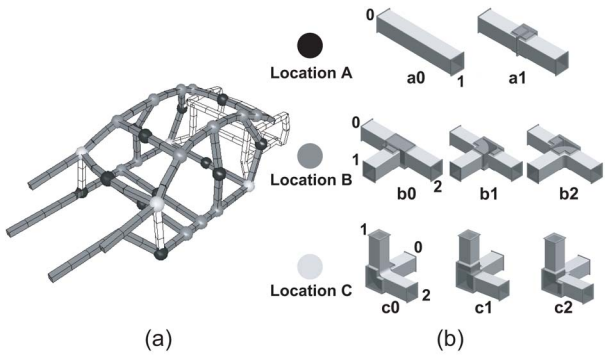

Fig. 13 (*a*) Possible joint locations and (*b*) feasible joint types at each location

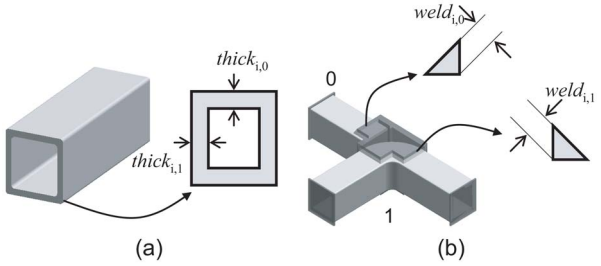

Fig. 15 Definitions of the beam cross-section design and welding design: (*a*) (thick$_{i,0}$, thick$_{i,1}$) $\in$ *FS$_i$*, the *i*th beam cross-section design used to define variable *y* (upper/lower thickness thick$_{i,0}$ and side thickness thick$_{i,1}$ and (*b*) (weld$_{i,0}$, weld$_{i,1}$) $\in$ *W$_i$*, the *i*th potential joint location welding design used to define variable *z* (weld thickness for component 0, weld$_{i,0}$ and for component 1, weld$_{i,1}$)

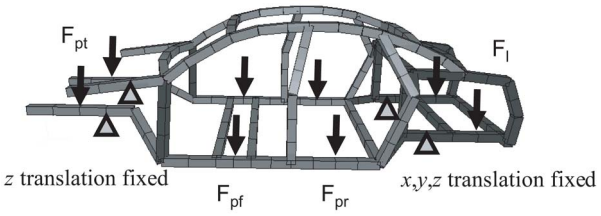

Fig. 16 Loading and boundary conditions [33]

Table 2 Applied load and dynamic load factor (one side)

	Default value (N)	Dynamic factor	Applied value (N)
F_{pt}	4000.0	2.0	8000.0
F_{pf}	1200.0	2.0	2400.0
F_{pr}	1200.0	2.0	2400.0
F_l	500.0	2.0	1000.0

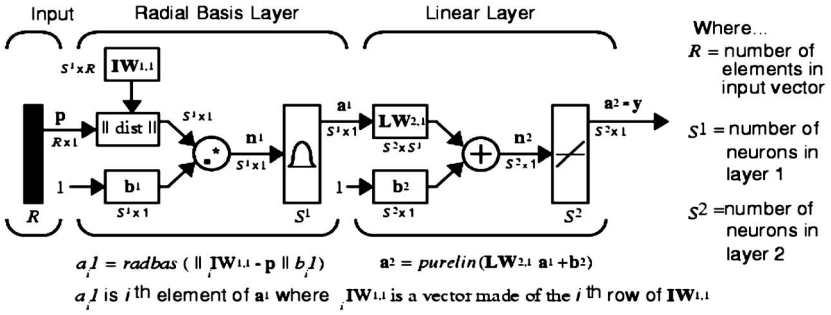

Fig. 17 Radial basis networks. In this case study, R=6, S^1=1250 and S^2=1 (adapted from [35]).

all joint types, a radial basis network [34] (Fig. 17) is built for each spring rate using the input vectors with six elements (four for two wall thickness of the two beam components and two for the two weld thicknesses in the joining sleeve), 1250 (=S^1 in Fig. 17) hidden layer nodes and 1 (=S^2 in Fig. 17) output node (joint rate). The networks are trained with NEWRB function in MATLAB [35] to reach a satisfactory convergence (rms error $<$ 10%).

The ASF model in this case study contains a total of 30 possible joint locations and 42 basic members. However, considering symmetricity reduces these to only 18 possible joint locations (12 in the left half and 6 at middle plane) and 21 basic members in the left half. Therefore, the chromosome $\boldsymbol{c}$ in Eq. (8) is composed of 96 elements by considering 18 for joint library, 42 (=21$\times$2) for beam cross-section designs, and 36 (=18$\times$2) for welding designs. Table 3 lists the parameter values for GAs used in the case study. The number of generation (100) was used as the termination condition. Using a PC with hyper-threaded Pentium 4 3.07 GHz, one optimization run takes approximately 4 days and 12 hr, mainly for about 50,000 FE analyses (each FE analysis takes about 7 s).

Figure 18 illustrates the convergence trend of the optimization run using 1,000 populations and 100 number of generation. Note that after a certain generation, the number of individuals in the Pareto Set converges to about 700 (70% of entire population). The termination condition used in this optimization is the specified terminal number of generation. However, this number should be determined based on the convergence trend.

Figure 19 shows the Pareto optimal solutions obtained at the terminal generation (=100). Figure 19(*a*) is the three-dimensional distribution of the 656 Pareto solutions (out of 1000 population). While all designs in the Pareto solutions are optimal in one sense, user or designer can select some designs that are mostly suitable for his/her interest. To better illustrate the trade-offs among the three objectives, Fig. 19(*b*) shows the solutions near f_{assm}= −57.5 projected on the $f_{\text{stiff}}-f_{\text{mfg}}$ plane, Fig. 19(*c*) shows the solutions f_{mfg}=−380.0 projected on the $f_{\text{stiff}}-f_{\text{assm}}$ plane, and Fig. 19(*d*) shows the solutions near $f_{\text{stiffness}}=-2.4\times10^{-3}$ projected on the $f_{\text{mfg}}-f_{\text{assm}}$. Three designs A, B, and C are selected on these "sliced" plots are shown in Fig. 20, and their objective function values are listed in Table 4.

Design A (Fig. 20(*a*)) shows good results both in stiffness and assembleability. This structure has components with relatively complex 3D geometries in the rear cabin (C1) and a long one-piece roof rail (C2), which gives a high rigidity in the structure.

Table 3 GA Parameter values used in the case study

Parameters	Value
Number of generation	100
Number of population	1000
Replacement rate (m/n)	0.5
Crossover probability	0.9
Mutation probability	0.1

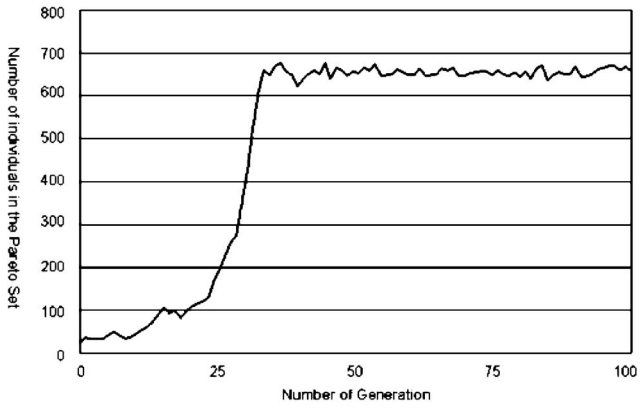

Fig. 18 Convergence trend of the optimization run for case study using 100 numbers of generation with 1000 numbers of population. Note that after a certain number of generation, number of individuals in the Pareto set converges to about 70% of the entire population.

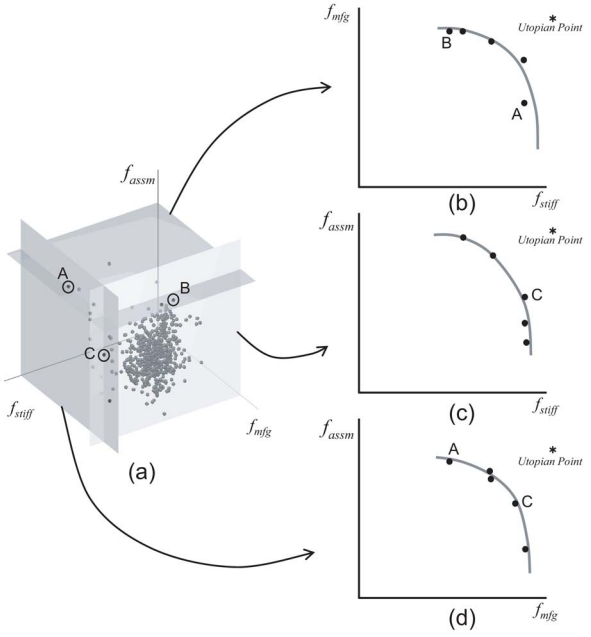

Fig. 19 (*a*) Pareto solutions at generation=100. Total 656 individuals among 1000 population are in the Pareto set. (*b*) Pareto solutions near f_{assm}=−57.5. (*c*) Pareto solutions near f_{mfg}= −380.0. (*d*) Pareto solutions near $f_{\text{stiff}}=-2.4\times10^{-3}$. Utopian points are located at the upper right corner of each graph.

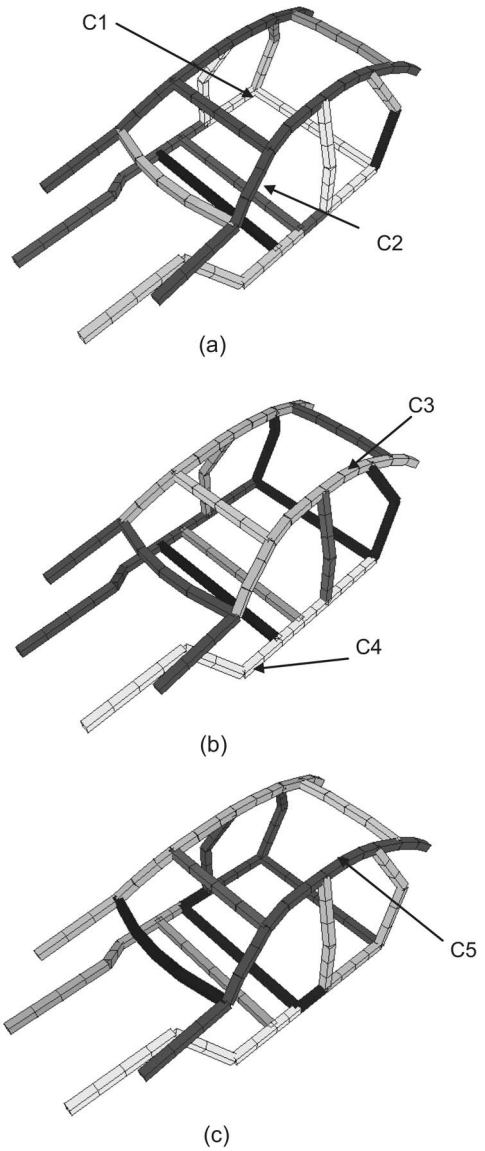

Fig. 20 Designs selected in the Pareto results in Fig. 19: (*a*) Design A (14 components) with good stiffness and assembleability, (*b*) design B (12 components) with good manufacturability, and (*c*) design C (12 components) balanced in all three objectives

Also, this design minimizes number of joint casting components by not having joints at location type A (see Fig. 13), resulting in good assembleability. However, relatively large numbers of components increases the extrusion die costs. Also, complex components with more bending increased the manufacturing cost.

Design B (Fig. 20(*b*)) shows good manufacturability. This design contains a minimum possible number of components (12) with the given joint library, which minimized the extrusion die costs. Also, relatively large but simple components (C3 and C4) reduced bending, resulting in good manufacturability. Design C (Fig. 20(*c*)) exhibits a relatively balanced result in all three objectives. It contains one-piece roof rail component (C5) as did design A, which gave this structure high rigidity. Also, by having minimum number of components (12) as in design B, and having relatively straight components it reduced the manufacturability cost.

Table 4 Objective function values for Design A–C

	No. Comp.	f_{stiff} (mm)	f_{mfg} ($)	f_{assm} ($)
A	14	**–0.002**	–510.0	**–69.08**
B	12	–0.155	**–360.0**	–71.36
C	12	–0.003	–380.0	–79.52

5 Summary and Future Work

This paper described a method for synthesizing multicomponent assemblies of a frame structure using a joint library. The problem is posed as a simultaneous determination of the locations and types of joints in a structure and the cross sections of the joined structural frames, considering structural characteristics, manufacturability, and assembleability. Multiobjective genetic algorithm, combined with direct crossover and FE analyses, is utilized. As a case study, a simplified model of the AFS body structure of a commercial vehicle is optimally decomposed into components. Three representative designs among the resulting Pareto solutions are examined, and their design characteristics and the trade-offs among the three objectives are discussed.

The following are the topics to be considered for future research: (i) adding objective functions for dimensional adjustability [11], (ii) expanding the joint libraries, (iii) integrating the "basic member library" to allow more diverse frame cross-sectional geometries for basic members, and (iv) using different multiobjective optimization algorithms besides the GAs.

Acknowledgments

The authors acknowledge funding provided by Toyota Motor Corporation and National Science Foundation under CAREER Award (DMI-9984606) for this research. We thank Karim Hamza at Discrete Design Optimization Laboratory at the University of Michigan for providing his FEM code. Any opinions, findings, and conclusions or recommendations expressed in this material are those of the authors and do not necessarily reflect the views of the National Science Foundation.

References

[1] Lyu, N., and Saitou, K., 2002, "Decomposition-Based Assembly Synthesis for Structural Stiffness," J. Mech. Des., **125**, pp. 452–463.
[2] Lyu, N., and Saitou, K., 2003, "Decomposition-Based Assembly Synthesis of a 3D Body-in-White for Structural Stiffness," *Proc. of 2003 ASME IMECE and R&D Exposition*, Washington, D.C., IMECE2003-43130, An extended version has been accepted to ASME J. Mech. Des..
[3] Cetin, O and Saitou, K., 2003, "Decomposition-Based Assembly Synthesis of Multiple Structures for Minimum Production Cost," *Proc. of 2003 ASME IMECE and R&D Exposition*, Washington, DC, ASME, New York, ASME Paper No. IMECE2003-43085.
[4] Jenkins, W. M., 1995, "Neural Network-Based Approximations for Structural Analysis," *Developments in Neural Networks and Evolutionary Computing for Civil and Structural Engineering*, Civil-Comp Press, Edinburgh, UK, pp. 25–35.
[5] Kang, H. T., and Yoon, C. H., 1994, "Neural Network Approaches to Aid Simple Truss Design Problem," Microcomput. Civ. Eng. **9**, pp. 211–218.
[6] Long, L., 1998, Design-oriented Translators for Automotive Joints, Ph.D. Thesis, Virginia Polytechnic Institute.
[7] Deb., K., Agrawal, S., Pratab, A., and Meyarivan, T., 2000, "A Fast Elitist Non-Dominated Sorting Genetic Algorithm for Multi-Objective Optimization: NSGA-II," KanGAL Report 200001, Indian Institute of Technology, Kanpur, India.
[8] Pereira, F., Machado, P., Costa, E., and Cardoso, A., 1999, "Graph Based Crossover—A Case Study With the Busy Beaver Problem," *Proc. of 1999 Genetic and Evolutionary Computation Conf.*, Orlando, Morgan Kaufmann, San Francisco, California, pp. 1149–1155.
[9] Lyu, N., and Saitou, K., 2003, "Topology Optimization of Multi-component structures via Decomposition-based assembly synthesis," *Proc. of 2003 ASME DETC*, Chicago, ASME, New York, ASME Paper No. DETC2003/DAC-48730 (an extended version accepted by J. Mech. Des.).
[10] Boothroyd, G. and Dewhurst, P., 1983, *Design for Assembly Handbook*, University of Massachusetts, Amherst, MA.
[11] Boothroyd, G., Dewhurst, P., and Knight, W., 1994, *Product Design for Manufacturing and Assembly*, Marcel Dekker, New York.
[12] Gupta, S. K., Regli, W. C., and Nau, D. S., 1994, "Integrating DFM With CAD

Through Design Critiquing," Concurr. Eng. Res. Appl., **2**, pp 85–95.
[13] Yetis, A., and Saitou, K., 2002, "Decomposition-Based Assembly Synthesis Based on Structural Considerations," J. Mech. Des., **124**, pp. 593–601.
[14] Lee, B., and Saitou, K., 2003, "Assembly Synthesis With Subassembly Partitioning for Optimal In-Process Dimensional Adjustability," *Proc. of 2003 ASME DETC*, Chicago, ASME, New York, ASME Paper No. DETC2003/DAC-48729.
[15] Chang, D., 1974, "Effects of Flexible Connections on Body Structural Response," SAE Trans., **83**, pp. 233–244.
[16] Lee, K., and Nikolaidis, E., 1992, "A Two-Dimensional Model for Joints in Vehicle Structures," Comput. Struct., **45**(4), pp. 775–784.
[17] Kim, Y. Y., Yim, H. H., and Kang, J. H., 1995, "Reconsideration of the Joint Modeling Technique: In a Box-Beam T-Joint," SAE Technical Paper No. 951108, pp. 275–279.
[18] Kim, Y. Y., and Kim, H., J., 2002, "New Accurate Efficient Modeling Techniques for the Vibration Analysis of T-Joint Thin-Walled Box Structures," Int. J. Solids Struct., **39**, pp. 2893–2909.
[19] Nishigaki, H., Nishiwaki, S., and Kikuchi, N., 2001, "First Order Analysis—New CAE Tools for Automotive Body Designers," SAE Technical Paper No. 2001-01-0768, *Proc. of SAE 2001 World Congress*, Detroit, SAE, Warrendale, PA.
[20] Overhagh, W. H., 1995, "Use of Aluminum in Automotive Space Frame," SAE Technical Paper No. 950721, *Int. Congress and Exposition*, Detroit.
[21] von Zengen K.-H. and Leitermann, W., 1998, "Space Frame—Quo Vadis?" SAE Technical Paper No. 982401, *Int. Body Engineering Conf. and Exposition*, Detroit.
[22] Kelkar, A., Roth, R., and Clark, J., 2001, "Automobile Bodies: Can Aluminum be an Economical Alternative to Steel?" JOM, **53**(8), pp. 28–32.
[23] A. Kelkar, 2001, Analysis of Aluminum in Auto Body Designs and its Strategic Implications for the Aluminum Industry, M.S. thesis, MIT, Boston.
[24] Honda Automotive Company, www.honda.com.
[25] Audi AG, www.audi.com.
[26] BMW, www.bmw.com.
[27] Ahmetoglu, M. A., 2000, "Manufacturing of Structural Automotive Components from Extruded Aluminum Profiles," SAE Technical Paper No. 2000-01-2712, *Int. Body Engineering Conf.*, Detroit.
[28] Chung, T., Lee, Y., and Kim, C., 1995, "Joint Design Approach for Aluminum Space Frame," SAE Technical Paper No. 950577, *Int. Congress and Exposition*, Detroit.
[29] Powell, H. J., and Wiemer, K., 1999, "*Joining Technology for High Volume Manufacturing of Lightweight Vehicles*," The Welding Institute, Cambridge, UK.
[30] Barnes, T. A., and Pashby, I. R., 2000, "Joining Techniques for Aluminum Spaceframes Used in Automobiles: Part I—Solid and Liquid Phase Welding," J. Mater. Process. Technol., **99**, pp. 62–71.
[31] Barnes, T. A., and Pashby, I. R., 2000, "Joining Techniques for Aluminum Spaceframes Used in Automobiles: Part II—Adhesive Bonding and Mechanical Fasteners," J. Mater. Process. Technol., **99**, pp. 72–79.
[32] Goldberg E. R., and Samtani M. P., 1986, "Engineering Optimization via the Genetic Algorithm," *9th Conf. on Electronic Computation*, New York, ASCE, pp. 471–82.
[33] Brown, J. C., Robertson, A. J., and Serpento, S. T., 2002, *Motor Vehicle Structures: Concept and Fundamentals*, SAE International, pp. 68–69.
[34] Chen, S., Cowan, C., and Grant, P. M., 1991, "Orthogonal Least Squares Learning Algorithm for Radial Basis Function Networks," IEEE Trans. Neural Netw., **2**(2), pp. 302–309.
[35] MATLAB, *The Language of Technical Computing*, 6.0.0.88, Release 12, The MathWorks.